Available online at www.sciencedirect.com
SCIENCE DIRECT®
Acta Materialia 53 (2005) 1831–1842
Acta MATERIALIA
www.actamat-journals.com

Strain hardening behavior of aluminum alloyed Hadfield steel single crystals

D. Canadinc [a], H. Sehitoglu [a,*], H.J. Maier [b], Y.I. Chumlyakov [c]

[a] *University of Illinois, Department of Mechanical and Industrial Engineering, 1206 W. Green St., Urbana, IL 61801, USA*
[b] *University of Paderborn, Lehrstuhl f. Werkstoffkunde, D-33098 Paderborn, Germany*
[c] *Siberian Physical-Technical Institute, Novosobornay Sq. 1, Tomsk, 634050, Russia*

Received 10 November 2004; received in revised form 21 December 2004; accepted 23 December 2004
Available online 25 January 2005

Abstract

Very high strain hardening coefficients (=G/23) are observed for aluminum-alloyed face-centered cubic Hadfield steel single crystals under tensile loading. Alloying with aluminum suppressed deformation twinning in two of the three crystallographic orientations studied, and transmission electron microscopy results revealed the existence of dense dislocation walls (sheets) along crystallographic directions that form barriers to slip deformation. A visco-plastic self-consistent algorithm was modified to account for the interaction between the active slip systems and the high density dislocation walls, producing close prediction of the experimental strain hardening response. The model predicted the added hardening in single crystals deformed along [$\bar{1}$ 1 1], [0 0 1] compared to the [$\bar{1}$ 2 3] orientation, the increase in volume fraction of the dislocation walls with increased deformation and the role of twinning in the [1 2 3] orientation.

Keywords: Hadfield steel; Strain hardening; Crystal plasticity; Microstructure; Dislocation walls

1. Background on strain hardening behavior of Hadfield steel

In previous work, the unusually high strain hardening coefficients of aluminum-free Hadfield steel have been attributed to the formation of twin boundaries that provided strong barriers to dislocation motion [1–7]. In addition, other reasons such as the dynamic strain aging, brought about by the reorientation of carbon members of C–Mn couples in the cores of dislocations, have been put forward to explain the unusual work hardening behavior [8]. Utilizing single crystals of Hadfield steel, Shtremel and Kovalenko [3] proposed that the strain hardening is caused by the interruption of the dislocation glide path by stacking faults. In another study on polycrystals of Hadfield steel, Zuidema et al. [9] investigated the role of aluminum on the strain hardening response, and demonstrated that addition of aluminum further increased the strain hardening rate. However, no detailed explanations of the role of aluminum on the stress–strain response have emerged, warranting a detailed look at the role of aluminum on deformation behavior of Hadfield steels.

In our previous studies [4–7,10] on single and polycrystals of Hadfield steel, using crystal plasticity concepts, we investigated the deformation behavior specifically addressing the interaction of twinning and slip deformation. The upward curvature in the stress–strain response was attributed to the increasing twin volume

* Corresponding author. Tel.: +1 217 333 4112; fax: +1 217 244 6534.
E-mail address: huseyin@uiuc.edu (H. Sehitoglu).

1359-6454/$30.00
doi:10.1016/j.actamat.2004.12.033

fraction providing a barrier to slip deformation. To decrease the role of stacking faults and twinning, aluminum was introduced to Hadfield steel to raise its stacking fault energy (SFE). Indeed in this case, the twinning is suppressed; however, a strain hardening coefficient higher (stress–strain response with an upward curvature) than that of the aluminum-free Hadfield steel was observed, motivating a closer study of this phenomenon. Our present work addresses the possible reasons for the observed strengthening prevalent in Al alloyed Hadfield steels.

We report experimental results for the stress–strain response and a modeling effort accounting for the slip system interactions making use of information on the microstructural processes obtained from transmission electron microscopy (TEM). The hardening is linked to the formation of high density dislocation walls (HDDWs) that form as a result of coplanar slip, and are oriented in the crystallographic $\langle 1\,1\,1\rangle$ directions. The number of such dislocation sheets depends on the single crystal orientation and the applied stress state. Although a model [11] has been proposed to predict the occurrence of such dense dislocation walls in early work on aluminum (and aluminum alloys), the role of these walls on the strain hardening response in single crystals has not been considered.

With respect to the high density dislocation walls (HDDWs), the most important previous modeling efforts concentrated on polycrystalline aluminum [11–13] and a steel in polycrystalline form with a body-centered cubic (bcc) crystal structure [14,15]. Extended Taylor algorithms were utilized to simulate the deformation response of these materials and to predict the corresponding texture evolution. The most significant contribution of these studies has been that they accounted for the influence of dense dislocation walls (also named dislocation sheets), that form by mutual trapping of glide dislocations, on the texture evolution. The utilization of single crystals in this study provides a clearer understanding of the contribution of the dislocation walls and the coupling between dislocation walls and active slip systems.

In the work presented herein, we pursue detailed experimental and numerical studies in order to improve the understanding of the role of dislocation sheet structures on the deformation response. We utilize single crystals where the slip directions and HDDWs are well defined. A crystal plasticity model is formulated that weighs the strengthening contributions from the dislocation wall domains and the matrix between the walls. A noteworthy observation is that the volume fraction of such dislocation walls increases with increasing deformation, effectively providing a barrier to further slip deformation, and an attendant increase in strain hardening rates. The choice of the single crystal orientations allowed one or more sets of dislocation walls to form, producing different levels of hardening. Overall, our combined experimental and modeling effort reported here elucidates the microstructural mechanisms, and provides a venue for incorporating the dislocation sheet structures in crystal plasticity.

2. Experimental techniques and results

The materials utilized in this study were Hadfield steel (with a chemical composition of 13.93 wt% Mn, 1.30 wt% C, and balance Fe) and aluminum alloyed Hadfield steel (13.93 wt% Mn, 1.30 wt% C, 2.58 wt% Al, and balance Fe). Both materials have face-centered cubic (fcc) crystal structure. The Bridgman technique was employed to grow single crystals on $\langle 1\,1\,1\rangle$ seeds in magnesia crucibles in a He atmosphere. Homogenization of the single crystals was carried out at 1323 K for 20 h. Electro-discharge machining was utilized to cut small-scale dogbone-shaped tension specimens.

A servohydraulic Instron 1331 test set-up equipped with an Instron 8500 controller was employed to perform the tests at room temperature with a strain rate of $4\times10^{-4}\,s^{-1}$. To check consistency between results, tests were repeated on three to six companion specimens. TEM was employed to observe the microstructure at several stages of deformation, and thereby relate the macroscopic changes to the relevant microstructural processes. For TEM analysis, 1 mm thick discs were sectioned with a low-speed diamond saw and then mechanically ground and polished down to about 120 μm thickness. Large electron transparent areas were obtained by conventional twin-jet polishing with an electrolyte consisting of 80 g anhydrous sodium chromate and 400 ml glacial acetic acid. All images analyzed in the present study were recorded after tilting the foils to the appropriate two-beam diffraction conditions.

The room temperature stress–strain response of Hadfield steel without aluminum (HS) and Hadfield steel with aluminum (HSwAl) are reported. We considered three different crystallographic orientations ($[\bar{1}\,1\,1]$, [0 0 1], and $[\bar{1}\,2\,3]$) under tensile loading. These orientations were selected to create different degrees of slip hardening and different sets of dislocation wall (sheet) structures.

The experiments revealed that the stress–strain response depends strongly on the crystallographic orientation, and is changed significantly with the addition of aluminum for all crystallographic orientations (Fig. 1). In Fig. 1(a) the results are given for Hadfield steel without aluminum and Fig. 1(b) depicts the results from the present study outlining the role of aluminum. The experimentally determined mechanical properties are given in Table 1. The addition of aluminum does not alter the

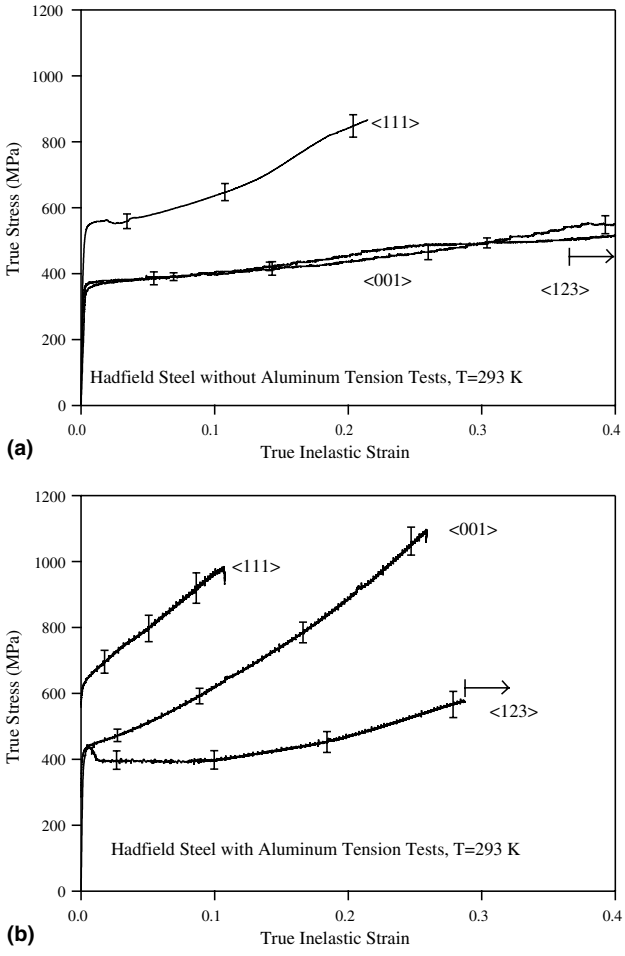

Fig. 1. True stress-true inelastic strain response of: (a) HS and (b) HSwAl for the $[\bar{1}\ 1\ 1]$, [0 0 1], and $[\bar{1}\ 2\ 3]$ orientation single crystals at room temperature under tensile loading. Tests ended with the failure of specimens. Arrows indicate that the corresponding specimens failed at a larger strain than shown here. The curves represent average of 3–6 tests. Strain hardening coefficients (normalized with respect to shear moduli) are given in Table 1.

critical resolved shear strength (Table 1). More significantly, the presence of Al increased strain hardening coefficient substantially for both $[\bar{1}\ 1\ 1]$ and [0 0 1] cases while the change in $[\bar{1}\ 2\ 3]$ orientation is rather small (Fig. 1). The deformation mechanisms (DM) depend on the crystallographic orientation and the alloy content. We note that twinning is observed for HS for $[\bar{1}\ 1\ 1]$ and [0 0 1] orientations while the deformation mechanism is predominantly slip in the HSwAl case.

The most significant effect of alloying with aluminum appeared to be the increased strain hardening observed for all orientations. This is reflected by the increase in the coefficients of strain hardening, especially with the [0 0 1] orientation. The strain hardening coefficients near $G/20$ to $G/30$ are considered to be rather high for fcc alloys. The $[\bar{1}\ 1\ 1]$ and [0 0 1] orientation single crystals of HSwAl demonstrated both a strengthening and an upward curvature at the onset of plastic deformation, and the $[\bar{1}\ 2\ 3]$ orientation HSwAl single crystals behaved in the same manner despite the initial softening at the early stages of the deformation. The $[\bar{1}\ 2\ 3]$ orientation also exhibits strain hardening at the later stages of the deformation. The formation of two sets of crystallographic boundaries (as in $[\bar{1}\ 1\ 1]$ and [0 0 1] orientations) has not been observed for the $[\bar{1}\ 2\ 3]$ case where single glide system is operative, rather only one HDDW set was apparent for this crystallographic orientation.

3. Microstructure

In order to gain an understanding of the microstructural evolution, TEM analysis was performed on the tested samples of all orientations. Based on the TEM results, the primary difference observed between HS and HSwAl single crystals is that twinning is suppressed in the $[\bar{1}\ 1\ 1]$ and [0 0 1] orientation single crystals of HSwAl and only micro twins are observed in the $[\bar{1}\ 2\ 3]$ orientation, whereas twinning and slip coexist in all crystallographic orientations for the HS case [4–7]. More importantly, the planar dislocation structures in the form of dislocation walls formed, thus providing effective obstacles against further dislocation motion in the HSwAl case (Figs. 2–4). These observations led us to construct a numerical model, which partly explains

Table 1
Critical resolved shear stress values (CRSS, MPa) at the onset of yielding, and coefficients of strain hardening (θ) (normalized with respect to shear moduli) for Hadfield steel single crystals utilized in this study

		⟨1 1 1⟩	⟨1 0 0⟩	⟨1 2 3⟩
HS	DM	Twinning	Multiple slip and twinning	Multiple slip and twinning
	SF	0.31	0.41	0.46
	CRSS (MPa)	159 ± 5	141 ± 3	162 ± 5
	θ	$G/40$	$G/170$	$G/91$
HSwAl	DM	Multiple slip	Multiple slip	Multiple slip and microtwins
	SF	0.27	0.41	0.46
	CRSS (MPa)	158 ± 4	154 ± 4	144 ± 5
	θ	$G/31$	$G/23$	$G/114$

DM, initial macro deformation mechanism; SF, Schmid factor; G, shear modulus.

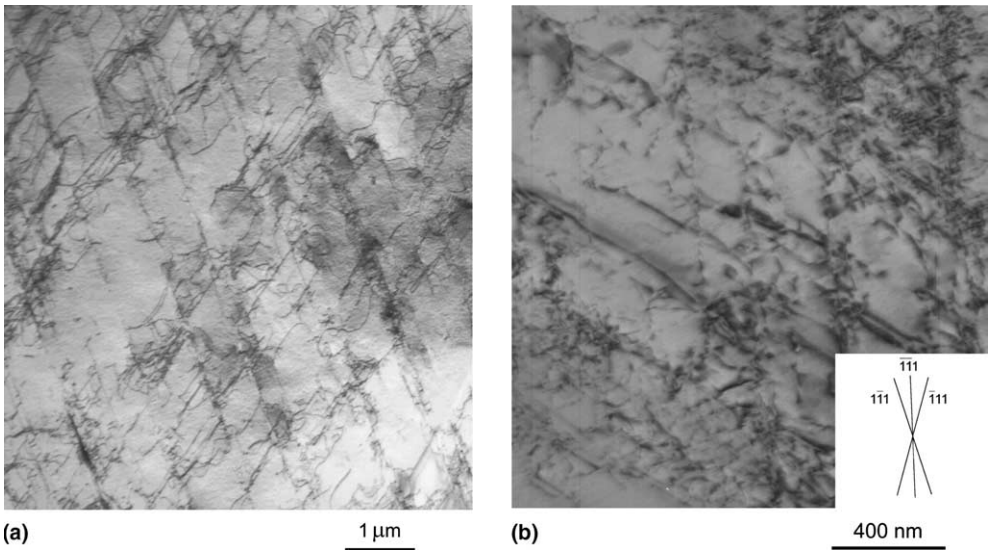

Fig. 2. (a) HSwAl [$\bar{1}$ 1 1] orientation subjected to 3% tensile strain. Low magnification overview showing two sets of dislocation sheet systems. (b) HSwAl [$\bar{1}$ 1 1] orientation subjected to 11% tensile strain. Traces of two planes, which are the planes of the active slip planes, are observed.

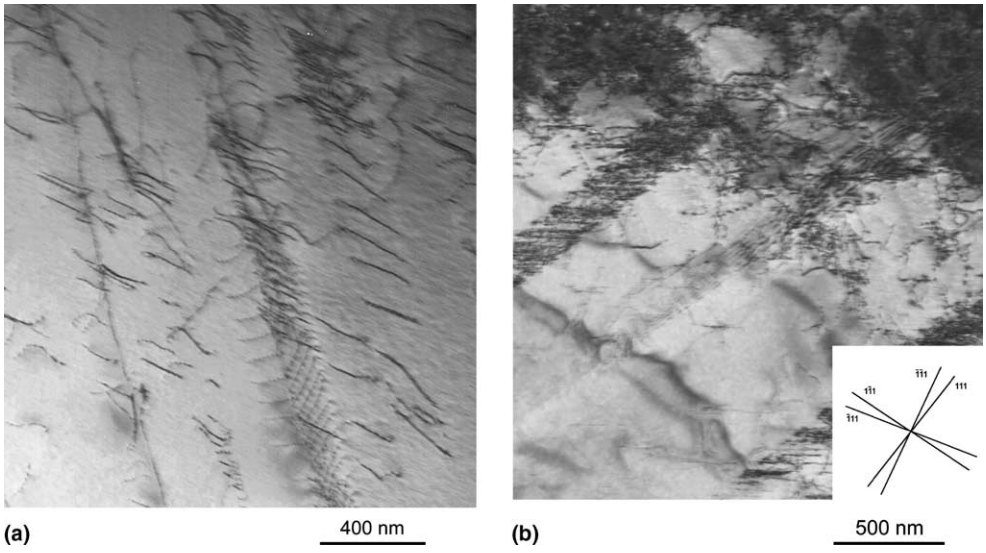

Fig. 3. (a) HSwAl [0 0 1] orientation subjected to 4% tensile strain. TEM image showing planar dislocation arrangements. (b) HSwAl [0 0 1] orientation subjected to 11% tensile strain. Traces of two active slip planes are observed.

the unusually high strain hardening behavior of HSwAl single crystals under tensile loading.

We observed dislocation sheets (with high dislocation densities) to form on planes corresponding to the most active slip systems. We identified two such dislocation arrangements in [$\bar{1}$ 1 1] orientated samples, two in [0 0 1] orientation, and one in [$\bar{1}$ 2 3] oriented single crystals of HSwAl (Figs. 2–4). In Figs. 2–4, the images labeled with (a) show the microstructure at early stages of plastic deformation. The insets labeled with (b) show the traces of the potential slip planes, for the individual sample orientations as obtained by conventional trace analysis. From the images it is apparent that a finite number of slip planes are activated. In Fig. 5, the activation of twin systems in addition to slip is evident for the [$\bar{1}$ 2 3] orientation at relatively small strain levels. Clearly, twinning plays a role in the stress–strain response for this orientation.

In summary, the present microstructural analysis demonstrates a planar slip structure in HSwAl single crystals. In general, decreasing SFE, increasing friction stress, increase in short range order (SRO) are known

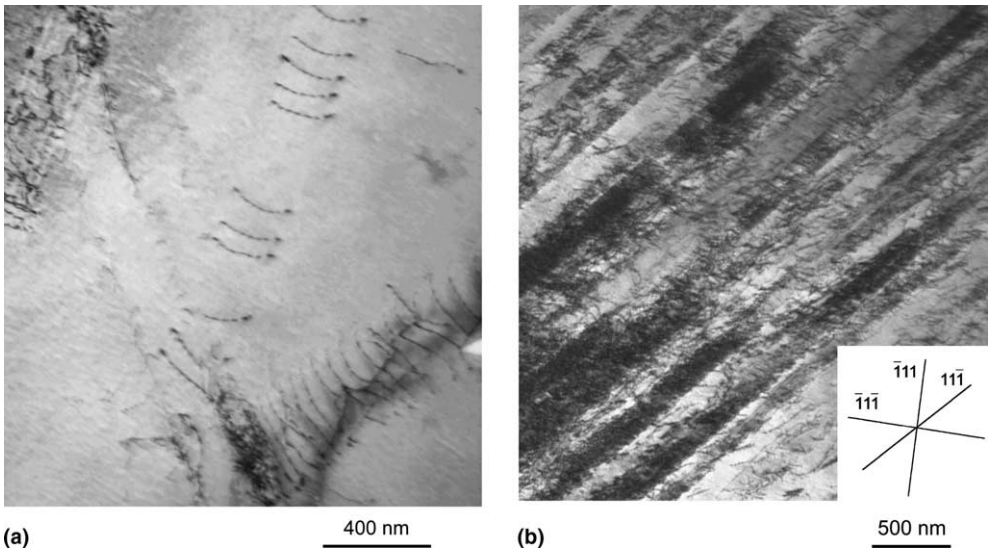

Fig. 4. (a) HSwAl [$\bar{1}$ 2 3] orientation subjected to 3% tensile strain. TEM image showing planar slip. (b) HSwAl [$\bar{1}$ 2 3] orientation subjected to 11% tensile strain. The trace of one set of dislocation sheet is observed. The second system is not well developed.

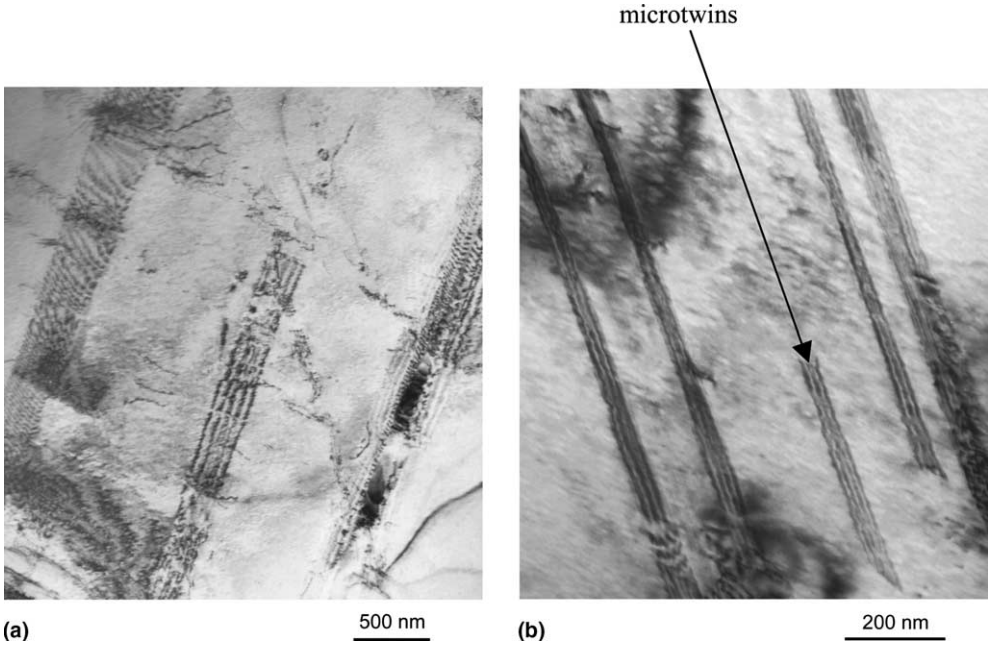

Fig. 5. (a), (b) HSwAl [$\bar{1}$ 2 3] orientation subjected to 3% tensile strain. Twins are evident at the early stages of deformation, showing that twinning (micro twins) was not totally suppressed in the [$\bar{1}$ 2 3] orientation due to aluminum addition. Although the structures shown in (a) may be mistaken with stacking faults, the contrasts do not fit to stacking faults.

to be the factors promoting the planarity of slip [12,16–19]. The addition of aluminum should increase SFE compared to HS, and thus should reduce slip planarity, however, this is not apparent based on the TEM observations. Clearly, the increase in SFE with aluminum is not sufficient to produce a change in the propensity of cross slip. Further work is needed to elaborate on the role of aluminum on the planarity of slip.

4. Modeling of stress–strain behavior: incorporation of slip system interactions into the numerical algorithm

Plastic deformation occurs when a slip or a twinning system becomes active. The resolved shear stress, τ^{s}_{RSS}, for a system (s) is given by

$$\tau^{s}_{RSS} = m^{s}_{i}\sigma_{i}, \tag{1}$$

where m_i^s is the vector form of the Schmid tensor and σ_i is the vector form of the applied stress. To describe the shear rate in the system, s, a non linear shear strain rate as a power of τ^s_{RSS} is written as,

$$\dot{\gamma}^s = \dot{\gamma}_0 \left(\frac{\tau^s_{RSS}}{\tau^s_0} \right)^n = \dot{\gamma}_0 \left(\frac{m^s_i \sigma_i}{\tau^s_0} \right)^n, \tag{2}$$

where $\dot{\gamma}_0$ is a reference rate, τ^s_0 is the threshold stress corresponding to this reference rate, and n is the inverse of the rate sensitivity index. If n is high enough, this description asymptotically approaches the rate insensitive limit. The total strain rate in a crystal can be written as the sum of all potentially active systems and can be pseudolinearized as follows [20],

$$\dot{\varepsilon}_i = \left[\dot{\gamma}_0 \sum_1^s \frac{m^s_i m^s_j}{\tau^s_0} \left(\frac{m^s_k \sigma_k}{\tau^s_0} \right)^{n-1} \right] \sigma_j = M^{c(sec)}_{ij}(\tilde{\sigma}) \sigma_j, \tag{3}$$

where $M^{c(sec)}_{ij}$ is the secant visco-plastic compliance of the crystal which gives the instantaneous relation between stress and strain rate.

Following Lebensohn and Tomé [20], at the polycrystal level the same pseudolinear form can be implemented as in the case of Eq. (3) as follows:

$$\dot{E}_i = M^{(sec)}_{ij}(\tilde{\Sigma}) \Sigma_j + \dot{\Sigma}^0, \tag{4}$$

where $\dot{E}_i$ and Σ are the polycrystal strain rate and applied stress.

Defining the deviations in strain rate and stress between the inclusion and the overall magnitudes as:

$$\tilde{\dot{\varepsilon}}_k = \dot{\varepsilon}_k - \dot{E}_k, \tag{5}$$

$$\tilde{\sigma}_j = \sigma_j - \Sigma_j, \tag{6}$$

and utilizing Eshelby's inhomogeneous inclusion formulation one can solve the stress equilibrium equation to derive the following interaction equation [21],

$$\tilde{\dot{\varepsilon}} = -\tilde{M} : \tilde{\sigma}. \tag{7}$$

The interaction tensor $\tilde{M}$ is defined as

$$\tilde{M} = n'(I - S)^{-1} : S : M^{(sec)}, \tag{8}$$

where $M^{(sec)}$ is the secant compliance tensor for the polycrystal aggregate and S is the visco-plastic Eshelby tensor [21].

The macroscopic secant compliance, $M^{(sec)}$, can be determined by substituting Eqs. (3) and (4) in Eq. (7). The macroscopic strain rate is evaluated by taking the weighted average of crystal strain rates over all the crystals as follows:

$$M^{(sec)} = \left\langle M^{c(sec)} : \left(M^{c(sec)} + \tilde{M} \right)^{-1} : \left(M^{(sec)} + \tilde{M} \right) \right\rangle. \tag{9}$$

Iterative solution of the Eqs. (3), (7) and (9) gives the stress in each crystal, the crystal's compliance tensor, and the polycrystal compliance consistent with the applied strain rate $\dot{E}_i$. In this work, we chose the term n (in Eq. (2)) to be in the rate insensitive limit ($n = 20$). As for the interaction Eq. (8), an effective value of $n' = 1$ is used.

It is known that the dislocation sheet structures contribute to the yield and flow stress anisotropy similar to texture effects in polycrystalline materials [12–15,19,22]. In these works, detailed microstructural analyses (TEM) revealed the existence of high-density dislocation sheets along with statistically stored dislocations and dislocations trapped in the high-density dislocation walls. Peeters et al. [14,15] showed that cell block boundaries (boundaries of dislocation cells with high dislocation densities) are formed parallel to the most active slip systems. They proposed an extended Taylor model accounting for the interaction of slip systems with each other and mobile dislocations in polycrystalline steel with a bcc structure. The high density dislocation sheets, also referred to as dense dislocation walls, were implemented into the model, such that they evolve and rotate in the crystal (grain) along with ongoing deformation. In the present experiments, we incorporate the increasing volume fraction of HDDWs by tracking their evolution with applied deformation, as well as the number of dislocation sheet sets as a function of crystallographic orientation of the specimens. Our aim is to predict the entire stress–strain response from small to large strains.

In the present work, we attribute the total hardening to two main components: the first accounts for the hardening due to dislocation motion and interaction of dislocations in the domains outside the HDDWs and the second due to HDDWs which act as effective obstacles to dislocation motion in the microstructure. The overall dislocation density can be expressed as

$$\dot{\rho} = \sum_n \left\{ k_1 \sqrt{\rho} - k_2 \rho \right\} |\dot{\gamma}^n| + \sum_n \sum_q \frac{K}{db} \cos\theta_{nq} |\dot{\gamma}^n|, \tag{10}$$

where k_1 and k_2 are constants, K is a geometric constant [4,10], α is the dislocation interaction parameter [23,24], and b represents the burgers vector (Table 2 lists the values of the constants used). The term $\sum_n \sum_q \frac{K}{db} \cos\theta_{nq} |\dot{\gamma}^n|$ accounts for the contribution due to the interaction between the dislocations on the active slip system n and the high density dislocation sheets formed parallel to the plane of the slip system q. The angle θ_{nq} is the angle between the direction of slip in the active slip system n and the normal to the plane of the slip system q. The term d represents the average spacing between the dislocation sheets.

We define the flow stress τ in the traditional Taylor hardening format as

$$\tau - \tau_0 = \alpha \mu b \sqrt{\rho}, \tag{11}$$

Table 2
Numerical values of constants used in the model

Constant	b (m)	d (m)[a]	ξ [26]	α [23,24]	K [4,10]	τ_0 (MPa)
Numerical value	2.58×10^{-10}	6×10^{-7}	0.4	0.4	8×10^{4}	159

ξ, α, and K are dimensionless quantities.
[a] An average value was assigned to this parameter based on the microstructural observations.

where τ_0 is a reference strength, which is taken as the microscopic yield in our analysis. The relationship between the term d, the average spacing between the HDDWs and the term f, that represents the volume fraction of HDDWs, is defined as follows:

$$\frac{1}{d}=\frac{1}{2t}\frac{f}{1-f}. \tag{12}$$

Here, the term t represents the average thickness of the high density dislocation sheets. From Eq. (11), with τ_0 constant, the rate of flow stress is obtained by taking the time derivative as

$$\dot{\tau}=\frac{\alpha\mu b\dot{\rho}}{2\sqrt{\rho}}. \tag{13}$$

Substituting Eq. (10) into Eq. (13) results in

$$\dot{\tau}=\frac{\alpha\mu\dot{\rho}}{2\sqrt{\rho}}\sum_n\left\{\frac{K}{db}\sum_n\cos\theta_{nq}+k_1\sqrt{\rho}-k_2\rho\right\}|\dot{\gamma}^n|, \tag{14}$$

which simplifies to

$$\dot{\tau}=\sum_n\left\{\frac{\alpha\mu K}{2d\sqrt{\rho}}\sum_n\cos\theta_{nq}+k_1\frac{\alpha\mu b}{2}-k_2\frac{\alpha\mu b}{2}\sqrt{\rho}\right\}|\dot{\gamma}^n|. \tag{15}$$

From Eq. (11), the following identity is obtained for the square root of the density of dislocations,

$$\sqrt{\rho}=\frac{\tau-\tau_0}{\alpha\mu b}. \tag{16}$$

Once the Eqs. (12) and (16) are substituted into Eq. (15), the rate of flow stress evolution is given by

$$\dot{\tau}=\sum_n\left[\frac{\alpha^2\mu^2bK}{4t(\tau-\tau_0)}\frac{f}{1-f}\sum_n\cos\theta_{nq}+\left\{k_1\frac{\alpha\mu b}{2}-k_2\frac{(\tau-\tau_0)}{2}\right\}\right]|\dot{\gamma}^n|. \tag{17}$$

One should note that the term $\{\frac{\alpha\mu b}{2}k_1-\frac{(\tau-\tau_0)}{2}k_2\}$ in Eq. (17) is the well-known Voce hardening term (see Eq. (22)). Having noted this, Eq. (17) can also be expressed as [21,25],

$$\dot{\tau}=\sum_n\left[\frac{\alpha^2\mu^2bK}{4t(\tau-\tau_0)}\frac{f}{1-f}\sum_n\cos\theta_{nq}+\left\{\theta_0\left(\frac{\tau_s-\tau}{\tau_s-\tau_0}\right)\right\}\right]|\dot{\gamma}^n|. \tag{18}$$

In this expression, θ_0 is the constant strain hardening rate, and τ_s represents the saturation stress in the absence of geometric effects, or the threshold stress. Nevertheless, the Voce type hardening alone falls short of accounting for the rapid strain hardening of the HSwAl, since it lacks the contribution of HDDWs to the hardening as impenetrable barriers in the matrix. This additional hardening due to the presence of HDDWs is included with the aid of the term,

$$\tau^B=2f\xi\mu\sum_n|\gamma^n|, \tag{19}$$

where the terms μ, ξ, and f stand for the shear modulus, the Eshelby accommodation factor (the contribution of high density dislocation sheets to the hardening is modeled as that of elongated ellipsoidal inclusions) [26], and the volume fraction of HDDWs, respectively. The $\sum_n\gamma^{(n)}$ term is simply the summation of the shear strains on the active slip systems and represents the total matrix mismatch strain brought about by the high density dislocation sheets. The influence of the rate of change of volume fraction of HDDWs is small compared to that of the shear rate on the rate of this particular hardening component, then Eq. (19) is expressed as follows in rate form,

$$\dot{\tau}^B=2f\xi\mu\sum_n|\dot{\gamma}^n|. \tag{20}$$

Combining Eqs. (20) and (18) yields the total rate of hardening, which is expressed as

$$\dot{\tau}=\sum_n\left[\frac{\alpha^2\mu^2bK}{4t(\tau-\tau_0)}\frac{f}{1-f}\sum_n\cos\theta_{nq}+2f\xi\mu+\left\{\theta_0\left(\frac{\tau_s-\tau}{\tau_s-\tau_0}\right)\right\}\right]|\dot{\gamma}^n|. \tag{21}$$

This model, basics of which have been derived in Eqs. (1)–(21), was implemented into the visco-plastic self-consistent (VPSC) code [20,21,25,27], by modifying the original version. The modifications were made in order to account for the additional contributions to hardening, and this modification procedure is explained in the following section, along with the other steps of the simulation procedure. The corresponding simulation results for the [$\bar{1}$ 1 1], [0 0 1] and [$\bar{1}$ 2 3] orientation single crystals are reported in comparison with the experimental results in Fig. 6. The simulations accurately predicted the stress–strain behavior of the HSwAl single crystals

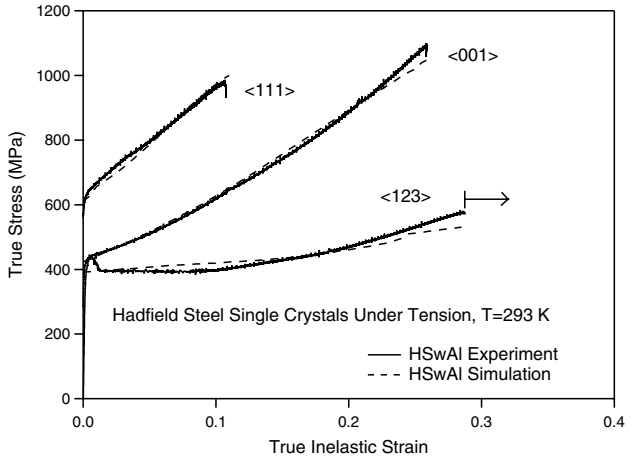

Fig. 6. Simulation results for the stress–strain behavior of single crystals of HSwAl in comparison with the corresponding experimental results. Arrow indicates that the corresponding specimen failed at a larger strain than shown here.

under tensile loading. Note that the deformation response of the single crystals of HS (without aluminum) is not simulated in this study as they were already successfully predicted in our previous studies [4–7].

The novelty of the modeling effort presented herein lies in the tackling of the problem of implementing the evolution of the HDDWs and their contribution to the hardening of the material. The original Code VPSC does not account for such structures and their influence on the deformation behavior.

In previous studies [4–7,10], we successfully modeled the slip-twin interactions using the capabilities of the Code VPSC. In the present study, we utilized a similar procedure to account for HDDWs (and their contribution to hardening) as adopted in twinning and twin reorientation schemes. In a recent study [10], we demonstrated the influence of twinning on hardening as hard boundaries that constitute an obstacle to dislocation motion. Based on these previous observations and modeling efforts, we modeled simultaneous evolution of HDDWs and mechanical twins on characteristic slip and twin planes with their respective volume fraction evolution. The HDDWs act as obstacles that block the dislocation motion, and part of these blocked dislocations become trapped and add to the density of HDDWs, fundamentally posing a similar barrier as twins with further straining.

We introduced the conventional trace analysis results into the VPSC algorithm in the form of plane normals and directions associated with the possible (1 1 1) planes that HDDWs form. As mentioned earlier, the HDDWs formed parallel to the planes of the most active slip systems, which was confirmed by our trace analysis. Therefore VPSC was given the normals of the sets of HDDW planes. Slip directions and slip planes for fcc crystal were also provided. The volume fraction at each step reflects the volume fraction of HDDWs, evolving along with increasing strain (Fig. 7). The results point to volume fraction of HDDWs evolving at a constant rate after some finite strain. It is expected that ultimately saturation of the density of dislocations trapped at the boundaries of HDDWs is expected but may not be observed because of the material failure.

In all calculations, the 12 $\langle 1\,1\,0\rangle$ (1 1 2) twin systems for twin evolution were included as an input, however they became prevalent only in the $[\bar{1}\,2\,3]$ case. We monitored the evolution of deformation twins, which were exhibited only by the $[\bar{1}\,2\,3]$ orientation single crystals for the HSwAl case (Fig. 5). Even before the numerical simulations were undertaken, the presence of slip as the dominant deformation mechanism in this orientation and the planarity of structures as in the other orientations indicated that the volume fraction of twins would not exceed a critical level, which is much less than the volume fraction of HDDWs in this orientation. The results point to approximately 4% as the volume fraction of twins, whereas 40% for the volume fraction of the HDDWs at 30% inelastic strain level in the $[\bar{1}\,2\,3]$ orientation single crystals of HSwAl (Fig. 7). Although the twin volume fraction is much less than that of HDDWs, the inclusion of twins (evident in Fig. 5) in the simulations of the $[\bar{1}\,2\,3]$ orientation allowed superior simulations of the stress–strain behavior. Once the twins were introduced, the crystallographic lattice orientation changes were influenced.

As the sample is strained, the HDDWs, which act as barriers to dislocation motion in the matrix rotate similar to the rotation of lattice slip systems. This was accounted for in our simulations as large strains (>10%) were realized. Our HDDW volume fraction evolution resemble that of twin volume fraction in the VPSC code,

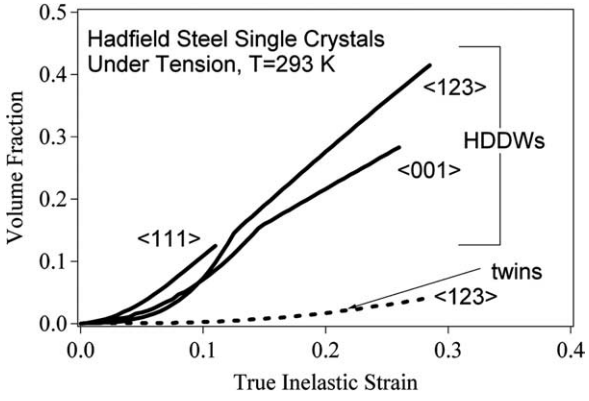

Fig. 7. Numerically calculated evolution of the volume fraction of HDDWs with respect to strain as a measure of increasing deformation. The twin volume fraction was also calculated for the orientation, which is the only crystallographic orientation that exhibits twins. We note that our model does not predict measurable twin volume fractions for the $[\bar{1}\,1\,1]$ and [0 0 1] cases, consistent with the experiments.

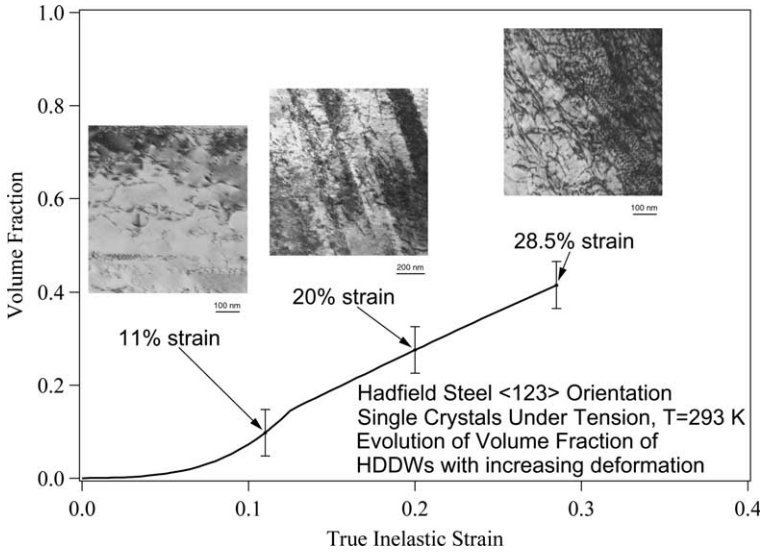

Fig. 8. A comparison of the experimentally measured and simulated volume fractions of HDDWs. TEM images recorded at different strains (from different specimens each strained to the specified levels) showing the increase in the density of dislocations trapped at the HDDWs with deformation. The $[\bar{1}\ 2\ 3]$ orientation is shown. The bars should not be confused with error bars, they indicate the strains at which the shown micrographs were recorded. The magnification bars of the TEM images reflect 100, 200, and 100 nm, from left to right.

albeit with different hardness and lattice planes. Therefore, at each step, the HDDWs increased in their dislocation densities and underwent continuous reorientation (Fig. 8). We note that HDDW volume fraction exceeds 40% at strains approaching 30%.

Having mentioned the key points in our model, it is appropriate to briefly go over the VPSC algorithm and the determination of the constants. The VPSC algorithm considers a polycrystalline aggregate and an initial texture information in the form of special orientations of the grains in this aggregate. This information is supplied to the Code VPSC as an input, which consists of three sets of Euler angles. In the simulation of single crystals, we considered the single crystals as polycrystalline aggregates [4–7,10] consisting of grains all of which have the same initial orientation in the Eulerian space. The Euler angles for each single crystal orientation were determined at the stage of single crystal growth and the cutting of different orientations out of these crystals [28].

The self-consistent algorithm is solved with three nested iterations [25]. Briefly, the outer iteration varies the stress and the compliance in each grain. The intermediate iteration varies the overall tangent modulus of the aggregate (see [27] for more details), whereas the inner iteration varies the overall secant compliance.

The hardening is defined by an extended Voce law [21,25], which is characterized by the evolution of the threshold stress (τ^s) with accumulated shear strain (Γ) in each grain of the form,

$$\tau^s = \tau_0 + (\tau_1 + \theta_1\Gamma)\left(1 - \exp\left(-\frac{\theta_0\Gamma}{\tau_1}\right)\right), \qquad (22)$$

where τ_0 is the reference strength (Table 2), and τ_1, θ_0 and θ_1 are the parameters that define the hardening behavior [21,25]. The original Voce hardening subroutine was modified, by implementing the additional terms given in Eq. (21).

Deformation is simulated by imposing successive strain increments. At each step, the boundary conditions are imposed to the aggregate. The boundary conditions are either the strain rate components, or a combination of strain rate and stress components. For grain reorientation, hardening and texture evolution, the algorithm employs the shear rates, whereas the macroscopic stress–strain components are given by volume averages over the grain components.

5. Final remarks and discussion

5.1. The role and importance of HDDWs

The unique feature of this study is the introduction of a new hardening approach in a visco-plastic self-consistent constitutive model incorporating the presence and volume fraction evolution of dislocation sheet structures, and their interaction with slip systems. The experimental stress–strain responses of single crystals of three different crystallographic orientations, and the experimental (TEM) observation of HDDWs constitute two separate critical checks of the validity of this new hardening approach.

It was mentioned earlier that several researchers previously concentrated on the influence of high density dislocation structures on the deformation response of

the materials studied [11–15,29,30]. While most of these studies considered polycrystalline materials, a limited amount of work is available on single crystals [30] motivating the present work. All these studies agree that dense dislocation wall structures form by mutual trapping of glide dislocations, and evolve and rotate with ongoing deformation. Our detailed microstructural analyses have confirmed the presence of such structures in Hadfield aluminum steels, and the proposed model is in good agreement with our microstructural findings and observations presented in this paper. Although, the deformation mechanism is predominantly slip the role of twinning has also been incorporated in our simulations.

In the present study, we specifically concentrated on the orientation dependence of the formation of the high density dislocation sheets facilitated by the use of single crystals. When the orientation dependence was investigated in previous work, however, the emphasis was mostly on texture of polycrystalline media. A detailed observation of the formation and, especially, the increase in volume fraction of the dislocation sheet structures had not been explored in single crystals, hence our detailed work on single crystals presented in this paper lays the foundation for further developments. The significance of the present model is the incorporation of the HDDWs and their interactions with the deformation mechanisms, and specifically their explicit evolution. The simulations revealed information not only about the volume fraction evolution of the high density dislocation sheets, and their rate of evolution being different depending on the orientation. It should be noted that, investigation of the orientation dependence was studied by both numerical simulations, and a detailed microstructural investigation utilizing TEM.

The interaction between the high density dislocation sheet structures and the active slip systems is treated as similar to the slip-twin boundary. In other words, the HDDWs are considered as impenetrable barriers to the dislocation motion and further slip on the systems interacting with them. Based on our TEM work, and supported by findings in the literature, the dislocations get trapped at the boundaries of the HDDWs that block the dislocation motion and glide, progressively increasing the volume fraction of these dislocation sheet structures. The present work provides a clear and detailed microstructural analysis (TEM), investigating the interaction between the slip systems and HDDWs utilizing a variety of crystallographic orientations at various stages of deformation (i.e., at different strain levels). Therefore, our description of incorporating the HDDWs and their influence on the deformation response into a visco-plastic self-consistent constitutive relationship proved to work satisfactorily, as our model successfully predicted the stress–strain behavior of HSwAl single crystals of selected orientations that represent different regions of the stereographic triangle.

The utilization of single crystals avoids the grain boundary effects and the related complexity of the micro-mechanisms defining the deformation behavior. Also, as shown in this work, the formation of HDDWs and the corresponding contribution to the hardening of the material is highly anisotropic. This implies a texture dependence in the case of polycrystalline versions of this material.

The focus of the paper has been the room temperature deformation of single crystals of Hadfield steels alloyed with aluminum. To isolate the role of HDDWs and their interaction with the slip systems on the overall deformation behavior we investigated cases where mechanical twinning is totally suppressed (and observed to small degree as in the case of $[\bar{1}\,2\,3]$ orientation). Therefore, the strain rate dependence of the deformation response is not included in this study. Instead, a low-to-average strain rate ($4\times10^{-4}\,s^{-1}$) was chosen to monitor the macroscopic stress–strain response and the corresponding changes in the microstructure. To reveal the strain rate and temperature dependence of the contribution of HDDWs to the stress–strain behavior of HSwAl single crystals, strain jump tests should be conducted at room temperature, and at both lower and higher temperatures. This will lay out the strain rate and temperature dependence of the formation and volume fraction of the high density dislocation sheet structures, but also constitute a separate check of the suppression of twinning with the addition of aluminum into the composition of Hadfield steel. Admittedly, these experiments are left aside for future research.

In a previous study, we examined the change of texture in the single and polycrystals of Hadfield steel [5] due to coexistence of slip and twinning as the deformation mechanisms. The comparison between the experimentally monitored and numerically calculated textural changes pointed at the success of our modification of the visco-plastic self-consistent constitutive relationship to account for the slip-twin interactions. In the present work, we focused on the formation and volume fraction evolution of the directional high density dislocation sheet structures in addition to their interaction with the active slip systems. It should be noted that the strains achieved due to tensile deformation of aluminum alloyed Hadfield steel are relatively large (exceeding 30%), especially in the case of $[\bar{1}\,2\,3]$ orientation single crystals. Large amount of straining is naturally expected to bring about a significant rotation of the crystal relative to the original crystallographic orientation, which implies a significant amount of change in the texture. The texture development is inevitably influenced by the presence and evolution of HDDWs. The results of Zakharova et al. [31] confirm such rotations with

a detailed study. However, their results point to the role of twinning at the earlier stages of deformation in all orientations, which was manifested only for the $[\bar{1}\ 2\ 3]$ orientation single crystals in this study and in the form of rather low volume fractions. Further work is necessary to understand how twinning is actually suppressed with additions of aluminum. The outcome of HDDWs and twinning is to produce upward curvature due to increased resistance to slip which opens potentially new applications for these alloys.

5.2. Determination of constants and hardening parameters

At this point, it is necessary to explain how the constants and hardening parameters were determined while trying to predict the room temperature stress–strain behavior of HSwAl single crystals. The determination of the fitting constants to be used in the model is a step by step procedure, rather than a trivial curve fitting process. The key is that, for the model to be declared as successful, the constants should be the same for all orientations, in addition to being physically meaningful, as they define the material's behavior in general.

For the present case, the $[\bar{1}\ 1\ 1]$ orientation was chosen to be the starting point. The first issue was the determination of the geometric fit constant K and the hardening parameters employed by the Voce hardening subroutine, such as τ_0, τ_1, θ_0 and θ_1. The τ_0 is defined as the reference strength, related to the measured yield strength (Table 2). The other three hardening parameters along with the geometric constant K of the Eq. (1), are determined while predicting the experimental deformation response that defines the stress–strain behavior of the $[\bar{1}\ 1\ 1]$ orientation single crystals.

Following the determination of the aforementioned fitting constants and hardening parameters for the $[\bar{1}\ 1\ 1]$ orientation, the same constants were utilized as an input to VPSC for the simulations of other two orientations. This procedure was repeated until the room temperature stress–strain responses of all orientations of the HSwAl were successfully predicted. At the end, most of the constants and parameters, including K, were approximately the same for all orientations, as well as the parameters θ_0 and θ_1.

Allowing a tensile (or compressive) stress in the $\langle 1\ 1\ 1\rangle$ direction of an fcc metal gives a corner in the 'plastic potential' as defined by Kocks and colleagues where the facets of six slip systems meet in the five-dimensional deviatoric stress space [21]. This means that six slip systems can be simultaneously activated, making the $\langle 1\ 1\ 1\rangle$ orientation a multi-slip orientation in fcc metals. Such highly symmetric situations are not possible with the other two orientations we studied for the fcc material case. Therefore, we chose the $[\bar{1}\ 1\ 1]$ orientation as the starting point for the determination of the fitting constants and hardening parameters, as the resulting parameters are more likely to capture the stress–strain behavior of the other orientations correctly. It should also be noted that, although the prediction of the stress–strain curve was the main path followed in the determination of constants and hardening parameters, we confirmed that the evolution of the HDDWs matched the microstructural observations, ensuring that our model captures the different hardening contributions.

6. Conclusions

In the present study, single crystals of Hadfield steel with and without aluminum have been investigated. We draw the following conclusions from this study.

1. The addition of aluminum to Hadfield steel (HSwAl) resulted in high strain hardening coefficients in $[\bar{1}\ 1\ 1]$ and [0 0 1] orientations attaining levels near $G/20$, while in the $[\bar{1}\ 2\ 3]$ case, the strain hardening and strengthening were similar to HS. The high levels of strain hardening coefficients in HSwAl single crystals were attributed to the high-density dislocation sheet arrangements, forming barriers to dislocation glide. Two sets of such boundaries were identified in the $[\bar{1}\ 1\ 1]$ and [0 0 1] cases while a single set of boundaries was present in the $[\bar{1}\ 2\ 3]$ case.
2. A VPSC (visco-plastic self consistent) code was modified to account for the number of dislocation sheets (HDDWs) formed along the crystallographic 1 1 1 planes and the contribution of these structures to the overall hardening, in an effort to model the room temperature stress–strain response of the single crystals of HSwAl. The volume fraction of such boundaries increased with deformation providing increased strengthening with accumulation of slip in single crystals. The increase in the volume fraction is consistent with extensive TEM findings.
3. The results presented confirm that crystallographic textural differences are not sufficient to explain the observed stress–strain response when dislocation boundaries with preferred orientations form. The evolution of such boundaries, with increased deformation, produces an additional anisotropy and strengthening. Specifically, the presence of multiple HDDWs led to higher hardening in the case of $[\bar{1}\ 1\ 1]$ orientation single crystals compared to the other two orientations studied.

Acknowledgements

This work was supported by the National Science Foundation Grant DMR-0313489. The authors are

grateful to Dr. Carlos Tomé for kindly offering the Code VPSC Version 5.0 to be modified in the modeling effort presented in this paper.

References

[1] Raghavan KS, Sastri AS, Marcinkowski MJ. Trans TMS-AIME 1969;245:1569.
[2] Adler PH, Olson GB, Owen WS. Metall Trans A 1986;17:1725.
[3] Shtremel MA, Kovalenko IA. Phys Met Metall 1987;63:158.
[4] Karaman I, Sehitoglu H, Gall K, Chumlyakov YI, Maier HJ. Acta Mater 2000;48:1345.
[5] Karaman I, Sehitoglu H, Beaudoin AJ, Chumlyakov YI, Maier HJ, Tomé CN. Acta Mater 2000;48:2031.
[6] Karaman I, Sehitoglu H, Chumlyakov YI, Maier HJ, Kireeva IV. Metall Mater Trans A 2001;32:695.
[7] Karaman I, Sehitoglu H, Chumlyakov YI, Maier HJ, Kireeva IV. Scripta Mater 2001;44:337.
[8] Dastur YN, Leslie WC. Metall Trans A 1981;12:749.
[9] Zuidema BK, Subramanyam DK, Leslie WC. Metall Trans A 1987;18:1629.
[10] Canadinc D, Karaman I, Sehitoglu H, Chumlyakov YI, Maier HJ. Metall Mater Trans A 2003;34:1821.
[11] Winther G, Juul Jensen D, Hansen N. Acta Mater 1997;45:5059.
[12] Hansen N, Juul Jensen D. Acta Metall Mater 1992;40:3265.
[13] Juul Jensen D, Hansen N. Acta Metall Mater 1990;38:1369.
[14] Peeters B, Kalidindi SR, Van Houtte P, Aernoudt E. Acta Mater 2000;48:2123.
[15] Peeters B, Seefeldt M, Van Houtte P, Aernoudt E. Scripta Mater 2001;45:1349.
[16] Hong SI, Laird C. Acta Metall 1990;38:1581.
[17] Owen WS, Grujicic M. Acta Mater 1999;47:111.
[18] Reed PR. JOM 1989:16.
[19] Winther G. In: Proceedings of the 19th Risø international symposium on materials science, Denmark; 1998. p. 185.
[20] Lebensohn RA, Tomé CN. Acta Metall Mater 1993;41:2611.
[21] Kocks UF, Tomé CN, Wenk HR. Texture and anisotropy. 2nd ed. Cambridge University Press; 2000.
[22] Raphanel JL, Schmitt JH, Baudelet B. In: Proceedings of the 19th Risø international symposium on materials science, Denmark; 1992. p. 491.
[23] Venables JA. J Phys Chem Solids 1963;25:693.
[24] Saada G. Acta Metall 1960;8:841.
[25] Lebensohn RA, Tomé CN. Manual for code visco-plastic self-consistent version 5; October 2002.
[26] Brown LM, Clarke DR. Acta Metall 1975;23:821.
[27] Turner PA, Tomé CN, Christodoulou N, Woo CH. Philos Mag A 1999;79:2505.
[28] Bunge HJ. Mathematische Methoden der Texturanalyse. Berlin: Akademie-Verlag; 1969.
[29] Liu Q, Juul Jensen D, Hansen N. Acta Mater 1998;46:5819.
[30] Liu Q, Hansen N. Phys Status Solidi A 1995;149:187.
[31] Zakharova EG, Kireeva IV, Chumlyakov YI, Maier HJ, Sehitoglu H. In: Proceedings of HNS 2004. Belgium: HNS; 2004.